Developing a 1D Axisymmetric Flow Profile in Liquid Mercury With Eddy Current Flow Meters and Deep Neural Networks

Grayson Gall[1] and Cornwall Lau[2]
[1)]*North Carolina State University*
[2)]*Oak Ridge National Laboratory*

(*Electronic mail: gsgall@ncsu.edu)

(*Electronic mail: lauch@ornl.gov)

(Dated: 11 August 2022)

Eddy Current Flow Meters (ECFMs) have been used to measure flows of conductive fluids for decades. Over the past decade or so, interest in ECFMs has increased due to applications in advanced fission reactors and possible applications in fusion reactors. ECFMs are well suited for such applications, as they can provide simple, compact, and external measurements of flow in fluids that are often high-temperature, corrosive and may contain radioisotopes. Traditionally, ECFMs are operated using an AC current at a single frequency. This operating condition has limited ECFMs to measure average fluid velocities, blockages, or voids in fluid channels. In this project, we set out to expand the capabilities of ECFMs by measuring the one-dimensional fluid velocity profile of liquid mercury in a pipe. To accomplish this, we made several ECFM sensitivity measurements at a range of frequencies. Different frequencies vary the electromagnetic skin depth of the device. Thus, by adjusting frequencies, we could probe the fluid velocity at various radial locations in the pipe and construct a radial flow-velocity profile. However, the relationship between the ECFM sensitivity measurements and the inferred velocity profile is highly nonlinear and requires solving an inverse problem. Traditional numerical methods for solving inverse problems are inefficient, numerically unstable, and require a unique solution for each ECFM frequency sweep. However, using electromagnetic finite-element simulations to train a Deep Neural Network, we were able to create a model that provides a general relationship between the sensitivity measurements of an ECFM and the fluid velocity profile with greater stability, for laminar, turbulent and monotonically decreasing flows in a pipe. Using the measured sensitivity in liquid mercury, our Deep Neural Network model calculates a flow profile that agrees well with computational fluid dynamic simulations of the flow profile. This technique has potential to improve real time flow monitoring for optimizing performance, ensuring safe operation of conductive fluid loops, and/or validating complex computational fluid dynamic models.

I. MOTIVATION

Alternating Current (AC) electromagnetic waves permeate materials to different depths depending on the AC frequency. The depth to which these waves permeate materials is called the skin depth. The electromagnetic skin depth for the ECFMs studied in this project is approximately proportional to the inverse of the square root of the AC frequency. Where σ is the permeability of the medium and ω is the AC frequency.

$$\text{Skin Depth} \sim \frac{1}{\sqrt{\sigma\omega}} \tag{1}$$

By varying the skin depth of the ECFM we can alter the radial location where the device is measuring the fluid velocity. Thus sampling over a range of frequencies gives us enough information to develop a fluid velocity profile in a pipe.

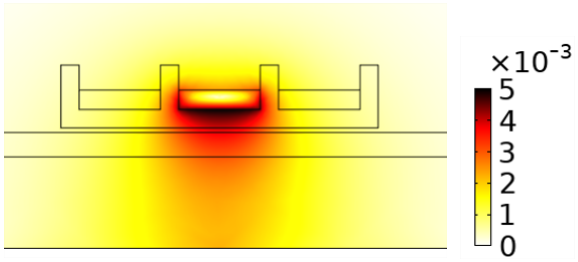

FIG. 1: Electromagnetic simulation of ECFM AC magnetic fields (T) with AC frequency at 50 Hz[1]

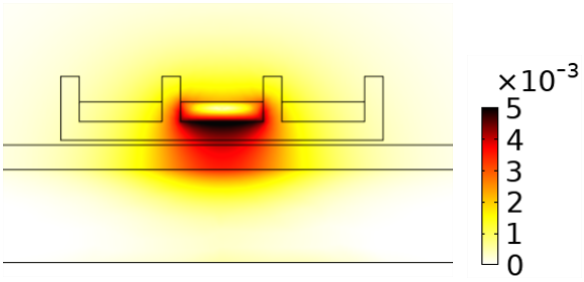

FIG. 2: Electromagnetic simulation of ECFM AC magnetic fields (T) with AC frequency at 1000 Hz[1]

II. METHODS

A. Problem Description

The forward relationship between ECFM sensitivity measurements and fluid velocity profile was developed with electromagnetic finite-element simulation in COSMOL using the assumption that the fluid velocity profile is the sum N rectangular functions. This yielded an MxN matrix, **A**, where M is the number of frequencies sampled with the ECFM and N is the number of radial locations where the fluid velocity is measured[1]. This forward relationship allowed us to generate sensitivity data from any arbitrary velocity profile with equation 2. Where $\vec{b}$ is an Mx1 vector of ECFM sensitivities, one at each of the M frequencies.

$$\mathbf{A}\vec{v} = \vec{b} \tag{2}$$

$\vec{b}$ is a measurable quantity vector so we set out to solve equation 3.

$$\vec{v} = \mathbf{A}^{-1}\vec{b} \tag{3}$$

B. Model Description

To solve equation 3 we used a fully connected Multi-Layer Perceptron Deep Neural Network (DNN). Where the input data was the sensitivity magnitude and phase and the output was the fluid velocity profile. In this application the DNN is effectively acting as $\mathbf{A}^{-1}$. A DNN was chosen for this problem for its ability to provide an efficient and stable general solution to equation 3.

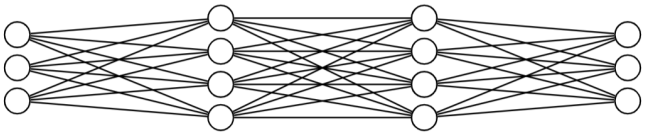

FIG. 3: Cartoon Representation of DNN used

Each DNN takes sensitivity magnitude and phase measurements at 13 different frequencies as input and returns the fluid velocity at 7 different radial locations.

Frequency Index	Frequencies Used [Hz]
1	200
2	500
3	1000
4	2000
5	3000
6	4000
7	5000
8	6000
9	7000
10	8000
11	9000
12	10000
13	12500

TABLE I: Table of frequencies at which ECFM measurements were taken

Position Index	Radial Location [cm]
1	0.32067
2	0.70548
3	0.83375
4	0.96203
5	1.07430
6	1.17050
7	1.25060

TABLE II: Table of radial positions where velocity was modeled by the DNN

C. Training Data Generation

Using the forward relationship, equation 2, generated with the COMSOL finite-element simulation[1,2] three DNNs were trained, each to predict a different type of velocity profile. Parabolic profiles, equation 5, were used to simulate laminar flow conditions. Power Law profiles, equation 7, were used to simulation turbulent flow conditions. Finally, Monotonically decreasing from the center of the pipe to the inner radius were used to simulate more general conditions. In order to generate a robust training set for the DNN to learn from, 8^7 flow profiles of each type were generated randomly for the training of each respective model.

1. Parabolic Data Generation

The formula used to simulate laminar flow is based on the analytic solution of the incompressible Naiver-Stokes equation in a cylindrical pipe[3].

$$v(r) = v_{\max}\left[1 - \left(\frac{r}{R}\right)^2\right] \tag{4}$$

A random minimum and maximum velocity, $v_{\min}$ and $v_{\max}$ were generated between 0 and 5 m/s and equation 4 was modi-

fied to guarantee that v_{max} occurred at the radial position closest to the center of the pipe r_{min}. Where r_{max} denotes the radial position closest to the wall of the pipe. The gives the form of equation 5, which was used to generate parabolic training data.

$$v(r) = \frac{v_{max} - v_{min}}{\left(1 - \left(\frac{r_{min}}{r_{max}}\right)^2\right)} \left[1 - \left(\frac{r}{r_{max}}\right)^2\right] + v_{min} \tag{5}$$

2. *Power Law Data Generation*

The formula used to simulate turbulent flow conditions is based on the Power Law approximation of a turbulent flow profile[4]. Where R is the inner radius of the pipe, we used $R = 1.2827$ cm.

$$v(r) = v_{max}\left(1 - \frac{r}{R}\right)^{1/n} \tag{6}$$

A random maximum velocity was generated in the range 0 to 5 m/s and a random value of n was chosen between 5 and 10. Equation 6 was then scaled such that the randomly generated maximum velocity v_{max} occurs at r_{min} giving the form of equation 7.

$$v(r) = \frac{v_{max}}{\left(1 - \frac{r_{min}}{R}\right)^{\frac{1}{n}}} \left(1 - \frac{r}{R}\right)^{\frac{1}{n}} \tag{7}$$

3. *Monotonically Decreasing Data Generation*

To simulate more general flow conditions a minimum and maximum velocity were randomly generated in the range 0 to 5 m/s. The remaining 5 velocity components were selected between those values such that velocity decreases with increasing radial position.

D. Uncertainty Quantification

Experimentally measured data is never perfect there is always some degree of error, noise, in real measurements. Because of this we needed to ensure that our model made accurate predictions with imperfect data. In order to do this we used the Monte Carlo Method. For a given sensitivity input a random 5% noise was put on each of the 13 magnitudes used by the model. The noise was generated by sampling a normal distribution with the probability distribution function given by equation 8 where the mean is the given sensitivity magnitude at the ith frequency, S_i, and the the standard deviation is 5% of the mean.

$$p_{n,i}(x) = \frac{1}{\sqrt{2\pi\sigma^2}} e^{\frac{(x-\mu)^2}{2\sigma^2}} \tag{8}$$

$$\mu = S_i \tag{9}$$

$$\sigma = 0.05\, S_i \tag{10}$$

This was done 1000 times for each model and then the Root Mean Squared Error (RMSE) and the Normalized Root Mean Squared Error (NRMSE) between the model predictions and correct velocity profile were calculated at each radial location. This Monte Carlo error analysis is intended to serve as an upper bound on the errors that may be possible with realistic levels of noise on experimentally measured data.

III. MODEL VERIFICATION

To verify that the model was working as expected a verification set of 2^7 profiles of the respective type were randomly generated. The velocity at each radial position of the model predictions was plotted against the correct velocity at the corresponding radial position. Then the difference in the predicted and correct velocity profiles was taken and plotted on a histogram. Models were trained and designed with the goal of having errors between ± 0.1 m/s between their predictions and the actual profiles in the verification data set.

A. Parabolic Model Verification

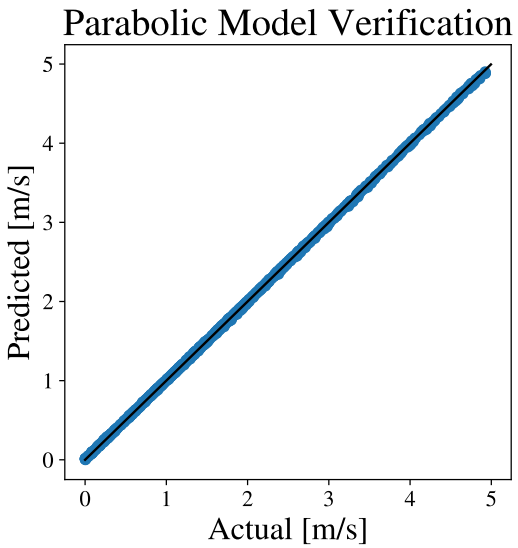

FIG. 4: Plot of DNN predictions of the verification data set versus the correct answers for the model trained with parabolic flow profiles

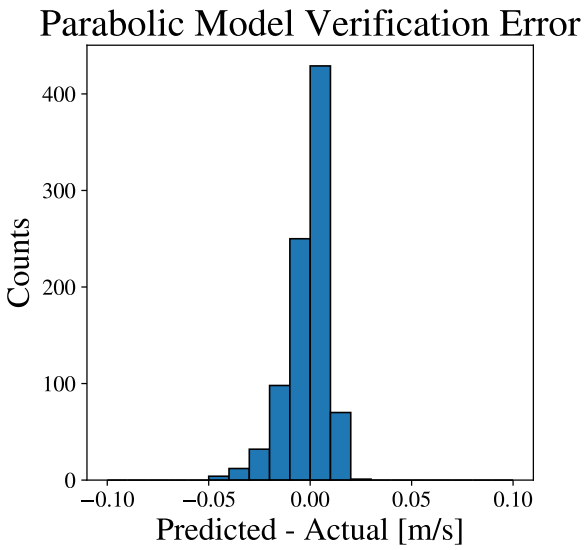

FIG. 5: Histogram of the error in the DNN predictions of the verification data set for the model trained with parabolic flow profiles

In both figures 4 and 5 we see that the parabolic model has generalized well. All errors between the model predictions and the actual profiles are less than ± 0.05 m/s, well within the ± 0.1 m/s goal.

B. Power Law Model Verification

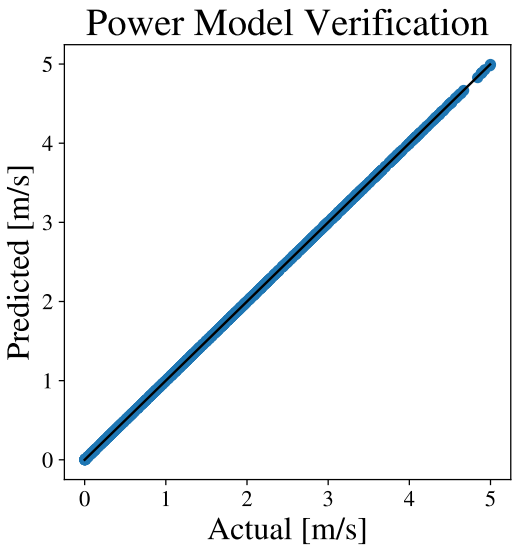

FIG. 6: Plot of DNN predictions of the verification data set versus the correct answers for the model trained with power law flow profiles

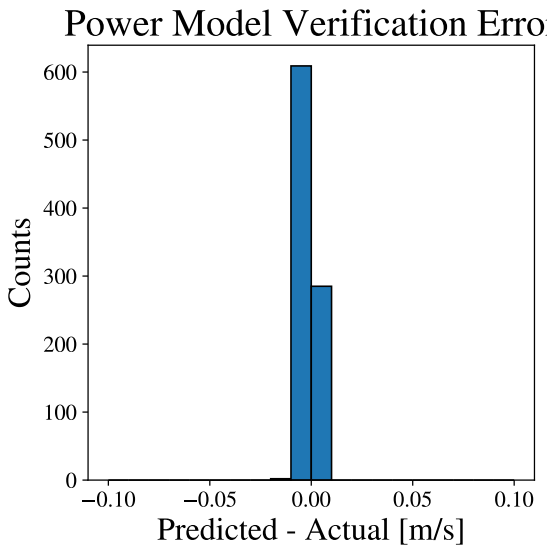

FIG. 7: Histogram of the error in the DNN predictions of the verification data set for the model trained with power law flow profiles

Similar to the model trained with parabolic flow profiles figures 6 and 7 indicate that the power law model has generalized well. However, in comparing figures 5 and 7 we can see that the power law model has significantly smaller error in its predictions than the parabolic model with all errors being between ± 0.015 m/s.

C. Monotonically Decreasing Model Verification

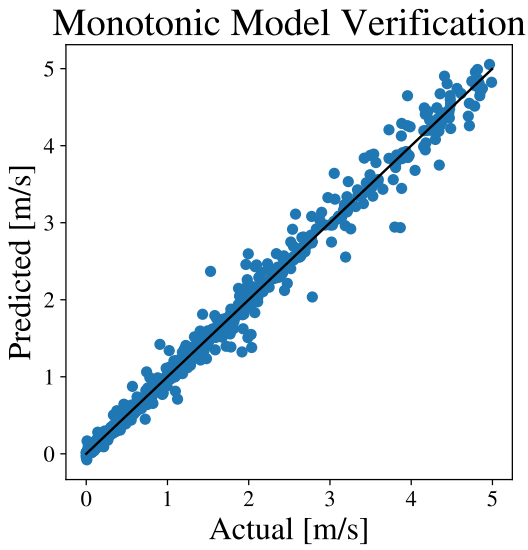

FIG. 8: Plot of DNN predictions of the verification data set versus the correct answers for the model trained with monotonically decreasing flow profiles

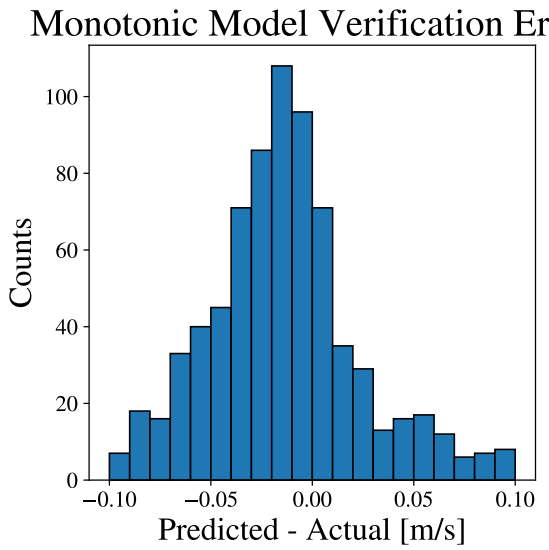

FIG. 9: Histogram of the error in the DNN predictions of the verification data set for the model trained with monotonically decreasing flow profiles

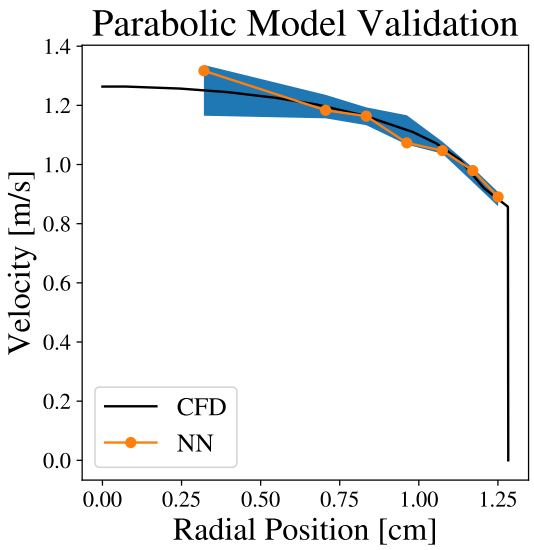

FIG. 10: Comparison of DNN predictions of flow profile using experimentally measured sensitivity and the CFD simulated flow profile. Using the DNN trained with parabolic flow profiles.

Figures 8 and 9 indicate that the monotonic model, while still successful in generalization did not generalize as well as the other two models. This, however, is to be expected as there is no analytic formula used in generating the flow profiles used for its training and verification. Despite this the overwhelming majority of the errors in its predictions are between ± 0.1 m/s. While there are some errors greater than the target threshold it is my belief that those outliers can be attributed to flow profiles that have extreme variation in the velocity between two neighboring radial locations. These may represent non-physical flow conditions and as such are not a point of concern.

IV. MODEL VALIDATION

To validate the DNN model, ECFM data[1] taken while the Test Target Facility was operating was used to make fluid velocity profile predictions. Those predictions were then compared to previous CFD simulations of the Test Target Facility liquid mercury loop[2]. Finally, the Monte Carlo uncertainty analysis discussed in section II D was used with the measured sensitivity data to better understand the stability of each models predictions. The models were trained and designed with the goal of having errors $\leq 10\%$ between the model predictions and the CFD simulated flow profiles using the measured data with the Monte Carlo uncertainty analysis.

A. Parabolic Model Validation

.

Position Index	AE [m/s]	NAE [%]
1	0.07	5
2	0.01	1
3	0.00	0
4	0.04	4
5	0.01	1
6	0.01	2
7	0.01	1

TABLE III: Table of Absolute Errors (AE) and Normalized Absolute Errors (NAE) between the DNN predictions using experimentally measured sensitivity and CFD simulated flow profile. Using the DNN trained with parabolic flow profiles.

Position Index	RMSE [m/s]	NRMSE [%]
1	0.09	7
2	0.04	3
3	0.03	2
4	0.05	4
5	0.02	2
6	0.02	2
7	0.02	2

TABLE IV: Table of errors in DNN predictions, using the measured sensitivity data with the Monte Carlo uncertainty analysis. Using the DNN trained with parabolic flow profiles

With the largest NRMSE in the parabolic models' predictions using the Monte Carlo uncertainty analysis being 7% and the actual errors in the prediction being at most 5% the DNN trained with the parabolic flow profiles shows good stability

and agrees well with the CFD simulated profiles. In figure 10 we can see that our model does not exactly match the curvature of the CFD simulated flow profile but rather predicts around it. I believe this to be caused by the fact that flow conditions in Test Target Facility are known to be in the turbulent regime[2]. With the model not seeing any turbulent flow examples it is expected that it may not capture the nuance of a turbulent flow profile. However, it does agree well with the CFD simulated profile in its trends and meets the stability and accuracy goals for this project.

B. Power Law Model Validation

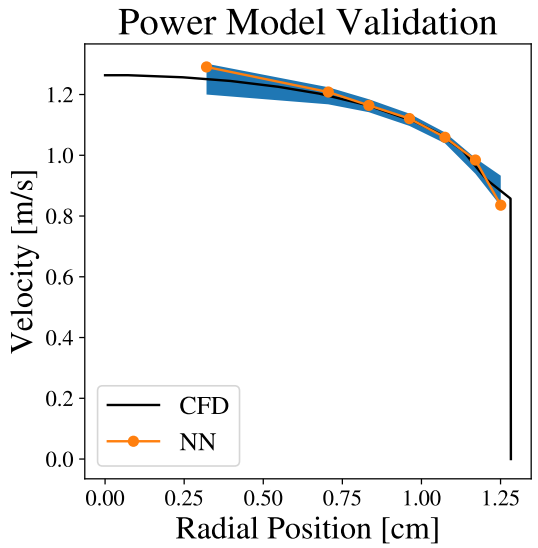

FIG. 11: Comparison of DNN predictions of flow profile using experimentally measured sensitivity and the CFD simulated flow profile. Using the DNN trained with power law flow profiles.

Position Index	AE [m/s]	NAE [%]
1	0.04	3
2	0.01	1
3	0.00	0
4	0.00	0
5	0.00	0
6	0.02	2
7	0.05	5

TABLE V: Table of errors between the DNN predictions using experimentally measured sensitivity and CFD simulated flow profile. Using the DNN trained with power law flow profiles.

Position Index	RMSE [m/s]	NRMSE [%]
1	0.05	4
2	0.03	2
3	0.02	2
4	0.02	2
5	0.02	1
6	0.02	2
7	0.05	4

TABLE VI: Table of errors in DNN predictions, using the measured sensitivity data with the Monte Carlo uncertainty analysis. Using the DNN trained with power law flow profiles

From figure 11 and tables III and VI we can see that the model trained with power law flow profiles performed well, both in terms of accuracy and stability. This result is to be expected. Since the model was trained to predict turbulent flow conditions it is no surprise that it performed well. This model is well within the stability requirements for this project and could potentially handle errors in measurements $\geq 5\%$ for these flow conditions.

C. Monotonically Decreasing Model Validation

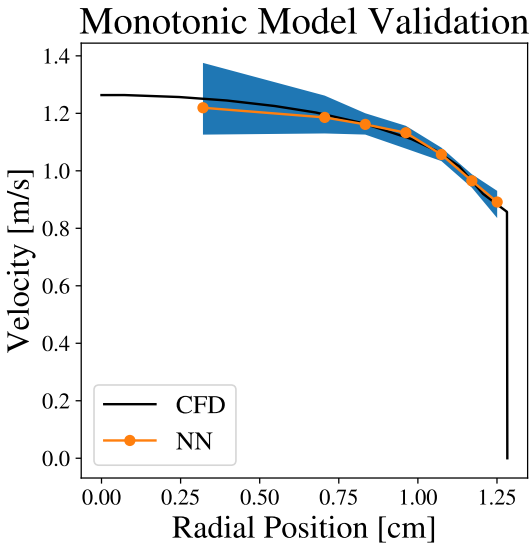

FIG. 12: Comparison of DNN predictions of flow profile using experimentally measured sensitivity and the CFD simulated flow profile. Using the DNN trained with monotonically decreasing flow profiles.

Position Index	AE [m/s]	NAE [%]
1	0.03	2
2	0.01	1
3	0.00	0
4	0.02	1
5	0.00	0
6	0.00	0
7	0.01	1

TABLE VII: Table of errors between the DNN predictions using experimentally measured sensitivity and CFD simulated flow profile. Using the DNN trained with monotonically decreasing flow profiles.

Position Index	RMSE [m/s]	NRMSE [%]
1	0.13	10
2	0.07	5
3	0.04	3
4	0.04	3
5	0.02	2
6	0.02	2
7	0.05	4

TABLE VIII: Table of errors in DNN predictions, using the measured sensitivity data with the Monte Carlo uncertainty analysis. Using the DNN trained with power law flow profiles

Interestingly the DNN trained with monotonically decreasing flow profiles agreed the best with the CFD simulated profile while also being the most unstable. This and other qualitative observations made while training the models suggests that there is a trade off between the generalization of the model and the stability. This is likely due to the fact that two completely different fluid flow profiles can have very similar sensitivity inputs and since there is no analytic formula for the profiles there is a larger pool of profiles that could have created those sensitivity inputs. However, the model only shows larger instabilities in predicting the fluid velocity closest to the center of the pipe. The model has very good stability and accuracy near the edge of the pipe where understanding the fluid behaviour is most important. Despite this larger instability near the center of the pipe the model still satisfies all stability requirements at every radial location.

V. CONCLUSION

By using ECFM sensitivity measurements coupled with DNNs we were able to extend the capabilities of ECFMs to accurately predict fluid velocity profiles. Predictions made by the DNN models with experimentally measured sensitivity data agreed well with CFD simulated velocity profiles regardless of the velocity profile type used to train the models. Errors in the DNNs predictions were also lower than those in ECFMs operated at a single AC frequency. The DNN models were also shown to be reasonably resilient to noisy input showing that this technique is one that could be used in practical applications. The particularly good performance of the power law model also suggests that using a model trained to predict flow in a systems known flow regime can increase accuracy and stability of ECFM flow profile measurements.

VI. FUTURE WORK

The development of an accurate and stable model for predicting 1D asymmetric fluid flow profile using ECFMs and DNNs gives the suggestion that with more complex ECFM geometry it may be possible to compose a 2D non-symmetric flow profile. However, this would require further electromagnetic simulation, ECFM design and possibly more advanced machine learning techniques to be applied. The work in this paper serves as a proof of concept that a diagnostic technique like this may be possible and worth pursuing.

A model with the ability to predict completely arbitrary flow profiles may also be of interest. While it is not mentioned in this report, this was attempted with little success. However, the model used in this work is quite basic and only uses two types of data as input. It may be possible to further expand this model with alternative/more advanced machine learning model structures and/or by including other relevant types of measurable ECFM data. This kind of capability would be of interest specifically for liquid metals flowing in tokamaks. Liquid metals in liquid breeder blankets for example would be subject to the influence of the strong magnetic fields that are used to confine the plasma. This can cause vortexes and highly irregular flow profiles in liquid metals[5]. So the ability to accurately measure these types of flows would of interest for the safe and efficient operation of these systems.

ACKNOWLEDGMENTS

This work was supported in part by the U.S Department of Energy, Office of Science, Office of Workforce Development for Teachers and Scientists (WDTS) under the Science Undergraduate Laboratory Internship (SULI) program.

This work was supported by Oak Ridge National Laboratory, managed by UT-Battelle. LLC for the US Department of Energy under DE-AC05-00OR22725.

[1] C. H. Lau, K. Oleksak, S. M. Cetiner, P. W. Groth, C. Mauer, D. D. Ottinger, M. J. Roberts, B. Warmack, and A. E. Fathy, "Eddy current flow meter model validation with a moving solid rod*," Measurement Science and Technology **33** (2022), 10.1088/1361-6501/ac6145.

[2] C. Lau, S. Cetiner, V. K. Varma, E. J. Fountain, P. Groth, C. Mauer, D. Ottinger, and B. Warmack, "Eddy current flow meter measurements and modeling validation," Tech. Rep. (Oak Ridge National Lab.(ORNL), Oak Ridge, TN (United States), 2022).

[3] P. Gerhart, A. Gerhart, and J. Hochstein, *Munson, Young and Okiishi's Fundamentals of Fluid Mechanics* (Wiley, 2016).

[4] H. Kudela, "Turbulent flow," (2010).

[5] L. Chen, S. Smolentsev, and M.-J. Ni, "Toward full simulations for a liquid metal blanket: part 2. computations of MHD flows with volumetric heating for a PbLi blanket prototype at Ha $\sim 10^4$ and Gr $\sim 10^{12}$," Nuclear Fusion **62**, 026042 (2022).